

Neutral Cr and V in the atmosphere of ultra hot jupiter WASP-121 b

MAYA BEN-YAMI,¹ NIKKU MADHUSUDHAN,¹ SAMUEL H. C. CABOT,² SAVVAS CONSTANTINOU,¹ ANJALI PIETTE,¹
SIDDHARTH GANDHI,^{3,4} AND LUIS WELBANKS¹

¹*Institute of Astronomy, University of Cambridge, Madingley Road, Cambridge CB3 0HA, UK*

²*Yale University, 52 Hillhouse, New Haven, CT 06511, USA*

³*Department of Physics, University of Warwick, Gibbet Hill Road, Coventry CV4 7AL, UK*

⁴*Centre for Exoplanets and Habitability, University of Warwick, Gibbet Hill Road, Coventry CV4 7AL, UK*

(Received 24 April 2020; Accepted)

ABSTRACT

Ultra hot jupiters (UHJs), giant exoplanets with equilibrium temperatures above 2000 K, are ideal laboratories for studying metal compositions of planetary atmospheres. At these temperatures the thermal dissociation of metal-rich molecules into their constituent elements makes these atmospheres conducive for elemental characterisation. Several elements, mostly ionized metals, have been detected in UHJs recently using high resolution transit spectroscopy. Even though a number of neutral transition metals (e.g., Fe, Ti, V, Cr) are expected to be strong sources of optical/NUV opacity and, hence, influence radiative processes in the lower atmospheres of UHJs, only Fe I has been detected to date. We conduct a systematic search for atomic species in the UHJ WASP-121 b. Using theoretical models we present a metric to predict the atomic species likely to be detectable in such planets with high resolution transmission spectroscopy. We search for the predicted species in observations of WASP-121 b and report the first detections of neutral transition metals Cr I and V I in an exoplanet at 3.6σ and 4.5σ , respectively. We confirm previous detections of Fe I and Fe II. Whereas Fe II was detected previously in the NUV, we detect it in the optical. We infer that the neutral elements Fe I, V I, and Cr I are present in the lower atmosphere, as predicted by thermochemical equilibrium, while Fe II is a result of photoionisation in the upper atmosphere. Our study highlights the rich chemical diversity of UHJs.

Keywords: Exoplanets — Hot Jupiters — Exoplanet atmospheres — Radiative transfer — Spectroscopy

1. INTRODUCTION

Ultra Hot Jupiters (UHJs) are emerging as promising laboratories for exploring the metal compositions of giant exoplanets. Due to their close proximity to their host stars these extremely irradiated gas giants have atmospheric temperatures of ~ 2000 – 4000 K, providing a unique opportunity to study planetary processes under extreme conditions, e.g., atmospheric escape (Ehrenreich et al. 2015; Yan & Henning 2018), day-night chemical variations (Wong et al. 2019; Ehrenreich et al. 2020) and thermal inversions (Haynes et al. 2015; Evans et al. 2017). Additionally, the molecules in such atmospheres

can be thermally dissociated into atoms and ions that can be observed using high resolution spectra (Kitzmann et al. 2018; Lothringer et al. 2018; Hoeijmakers et al. 2019).

In recent years, several metallic species have been detected in UHJs, predominantly through high resolution Doppler spectroscopy (e.g., Hoeijmakers et al. 2019; Casasayas-Barris et al. 2019). The detections are typically made using the cross-correlation method (Snellen et al. 2010), which has proven to be a robust way to detect molecular, atomic and ionic species in hot Jupiters in general (Snellen et al. 2010; Brogi et al. 2012; Birkby 2018; Hoeijmakers et al. 2019). The elemental detections include Na I, Mg I, Sc II, Ti II, Ca II, Cr II, Fe I, Fe II and Y II in KELT-9 b (Hoeijmakers et al. 2018, 2019; Cauley et al. 2019; Yan et al. 2019; Turner et al. 2020);

Na I, Ca II, Mg I, Cr II, Fe I and Fe II in MASCARA-2 b (Casasayas-Barris et al. 2019; Stangret et al. 2020; Nugroho et al. 2020; Hoeijmakers et al. 2020); Ca II in WASP-33b (Yan et al. 2019); and Na I, Fe I, Fe II, Mg II in WASP-121 b (Sing et al. 2019; Bourrier et al. 2020; Cabot et al. 2020; Gibson et al. 2020).

Most of the metal detections in UHJs to date are ions, with the exception of prominent species Na I, Mg I and Fe I, all of which have solar abundances above 1 ppm. On the other hand, the lower atmospheres of UHJs are expected to host a number of trace metals in neutral form (Kitzmann et al. 2018). In particular, trace transition metals (e.g., Ti I, V I, Cr I, Mn I) can be strong sources of optical/NUV opacity (Lothringer et al. 2020) and can provide important probes of physicochemical processes in the lower atmosphere, as discussed in Section 5.

Therefore, a consistent framework to determine a priori the detectability of atomic species would be valuable to inform observations and allow for comparative chemical characterisation of UHJs. We explore such an approach in the present work using the case study of WASP-121 b, an UHJ of considerable interest from recent studies (e.g. Delrez et al. 2016; Evans et al. 2017, 2018; Bourrier et al. 2020; Parmentier et al. 2018). Notably, it has been suggested to contain a thermal inversion (Evans et al. 2017). While TiO/VO are traditionally considered strong candidates for causing thermal inversions (Fortney et al. 2008) they have proved elusive in this planet (Evans et al. 2018; Mikal-Evans et al. 2019; Merritt et al. 2020), prompting considerations of other species (Lothringer et al. 2018; Gandhi & Madhusudhan 2019). Furthermore, its bright host star ($V = 10.44$) and inflated radius make WASP-121 b particularly amenable to atmospheric characterization. We consider a metric to predict the detectable atomic species in WASP-121 b based on their abundances in thermochemical equilibrium and the number and strength of their spectral lines. We then search for the predicted species in high resolution optical spectra of WASP-121 b, and confirm our predictions.

2. MODELLING AND THEORY

Here we explore the expected atomic composition and spectral signatures of UHJ atmospheres with WASP-121 b as our case study. We assess the prominent species with thermochemical equilibrium calculations, compute absorption cross-sections for these species and use these cross-sections to investigate optical transmission spectra of WASP-121 b.

2.1. Atomic Abundances

We examine the atomic abundances in the photospheres of UHJs under the assumption of thermochemical equilibrium. The chemical calculations were conducted using the HSC CHEMISTRY software (version 8)¹. We assumed solar elemental abundances (Asplund et al. 2009). The input species were expanded upon those used by Harrison et al. (2018) to include important molecular, atomic and ionic forms of the top 36 elements in solar abundance. Other similar calculations show the prominence of atomic species in UHJs (e.g., Kitzmann et al. 2018; Lothringer et al. 2018; Nugroho et al. 2020).

Although the equilibrium temperature of WASP-121b is ~ 2400 K, we expect its observed composition to be characteristic of the 2800 K temperatures at ~ 0.1 -1 bar (Gandhi & Madhusudhan 2019) due to strong vertical mixing (Parmentier et al. 2013). Figure 1 shows abundances of some prominent transition metals as a function of temperature at 0.1 bar. It can be seen that above ~ 2500 K these elements are primarily found in their neutral atomic form rather than in molecules. We thus take the total elemental abundance, which we have assumed to be solar, as a good approximation for the abundance of neutral atomic species above 2500 K.

2.2. Atomic Cross sections

We calculate atomic absorption cross sections for a large number of elements in order to investigate their spectral features. We rank the elements by their solar abundances (Asplund et al. 2009), excluding H, noble gases and halogens. We calculate the cross sections for all the neutral and singly ionised forms of the top 30 elements, following the methods of Gandhi & Madhusudhan (2017). We use atomic line lists provided by Kurucz (2018) similar to the approach in other recent studies (e.g., Hoeijmakers et al. 2018; Casasayas-Barris et al. 2019; Nugroho et al. 2020). We determine the partition functions from the energy levels and statistical weights from the NIST database (Kramida et al. 2018). We include the effect of thermal broadening of the atomic lines, but do not consider pressure broadening as high resolution spectra probe lower pressure regions in the upper atmosphere (Wyttenbach et al. 2015; Snellen et al. 2010). Our calculations do not include the effect of rotation and atmospheric expansion on the shape of the lines. All our models also include Rayleigh scattering from H_2 and collision-induced absorption (CIA) from H_2 - H_2 and H_2 -He (Richard et al. 2012). An example of

¹ www.hsc-chemistry.com

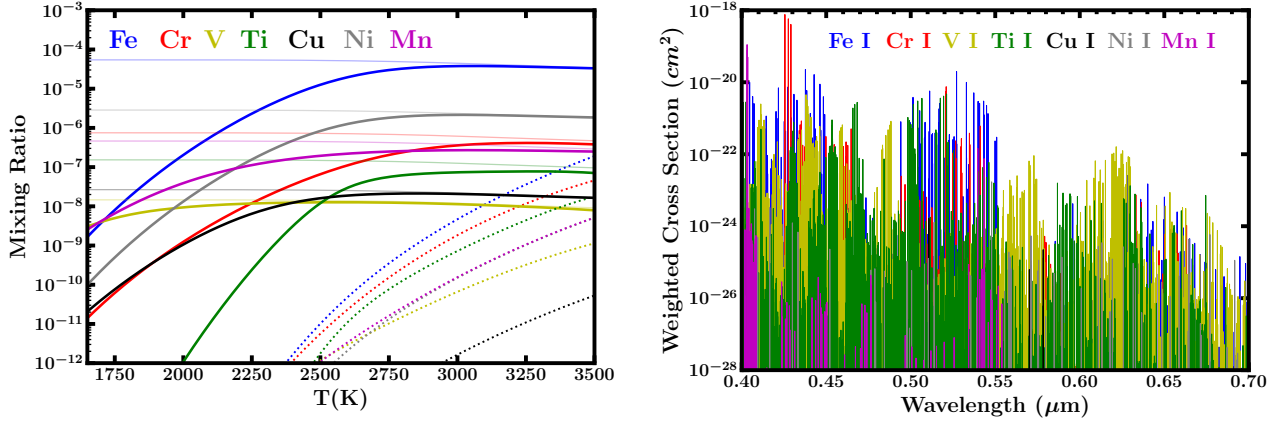


Figure 1. Equilibrium volume mixing ratio and absorption cross sections for several transition metals. *Left:* The solid (dotted) lines show the neutral (singly ionised) abundances as a function of temperature at 0.1 bar pressure assuming solar elemental abundances (Asplund et al. 2009); see section 2.1. The thin solid line for each species shows the mixing ratio it would have if all its elemental abundance was in neutral atomic form. *Right:* Absorption cross sections at 2000 K weighted by their solar elemental abundances.

these cross sections scaled by solar abundance for some prominent transition metals can be found in Figure 1.

2.3. Theoretical Spectra

We investigate the spectral signatures of the atomic species discussed above using both simple semi-analytic models as well as fully numerical models. First, we compute transmission spectra of WASP-121 b using the analytic formulation originally derived by Lecavelier Des Etangs et al. (2008) (also see e.g., de Wit & Seager 2013; Bétrémieux & Swain 2017). This prescription assumes an isothermal atmosphere with a uniform composition and a constant scale height. The wavelength dependent effective height of the atmosphere is given by:

$$h(\lambda) = H \ln \left(\frac{\sqrt{2\pi R_{pl} H n_0}}{\tau_{eq}} \sigma_{\text{total}} \right), \quad (1)$$

with total opacity

$$\sigma_{\text{total}} = \sum_i \chi_i \sigma_i(\lambda) + \sigma_R(\lambda) + n_0 \sigma_{\text{CIA}}(\lambda), \quad (2)$$

where σ_R is the opacity due to Rayleigh scattering, σ_i and χ_i are the absorption cross section and mixing ratio of species i , and $n_0 \sigma_{\text{CIA}}$ is the appropriately scaled CIA cross section. The CIA approximation in Equation 2 is adequate here considering that the CIA contribution in the optical is negligible. The scale height is given by $H = (k_B T) / (\mu g)$ where k_B is the Boltzmann constant, T is the temperature, μ is the mean molecular mass and g is the gravitational acceleration. R_{pl} is the planet continuum radius, n_0 is the number density at a given reference pressure P_0 , and $\tau_{eq} = 0.56$ (Lecavelier

Des Etangs et al. 2008). For a star of radius R_{star} the absorption spectrum is then:

$$\delta(\lambda) = \frac{(R_{pl} + h(\lambda))^2}{R_{\text{star}}^2} \quad (3)$$

We generate such analytic spectra for atomic species in the atmosphere of the ultra hot Jupiter WASP-121 b. We consider the contribution to the opacity of only one species j at a time, in addition to continuum opacity due to Rayleigh Scattering and CIA, to calculate the spectrum δ_{c+j} . Here χ_j is taken to be the solar elemental mixing ratio of the species j . The corresponding atomic cross sections are calculated at 2000 K as described in Section 2.2. Examples for Fe I, Cr I, V I and Ti I can be seen in Figure 2. We adopt the planet parameters from Delrez et al. (2016) as $R_p = 1.828 R_J$, $M_p = 1.183 M_J$, $R_{\text{star}} = 1.458 R_{\text{sun}}$. We assume $\mu = 2.22$ (similar to Jupiter), $P_0 = 0.1$ bar and $T = 2000$ K, and calculate the spectra from 0.4 to 0.7 μm with a resolution of $R = 10^5$. We use these analytic model spectra to compute our detectability metric for the different species, as discussed in section 4.1.

For the cross-correlation analyses we use fully numerical models to compute the transmission spectra for the species discussed above. We use an adapted version of the forward model in the AURA retrieval code (Pinhas et al. 2018). AURA computes line-by-line radiative transfer for a plane-parallel atmosphere in transmission geometry, assuming hydrostatic equilibrium. We assume uniform chemical abundances and an isothermal temperature profile at 2000 K. The sources of opacity and spectral range are the same as described above for the

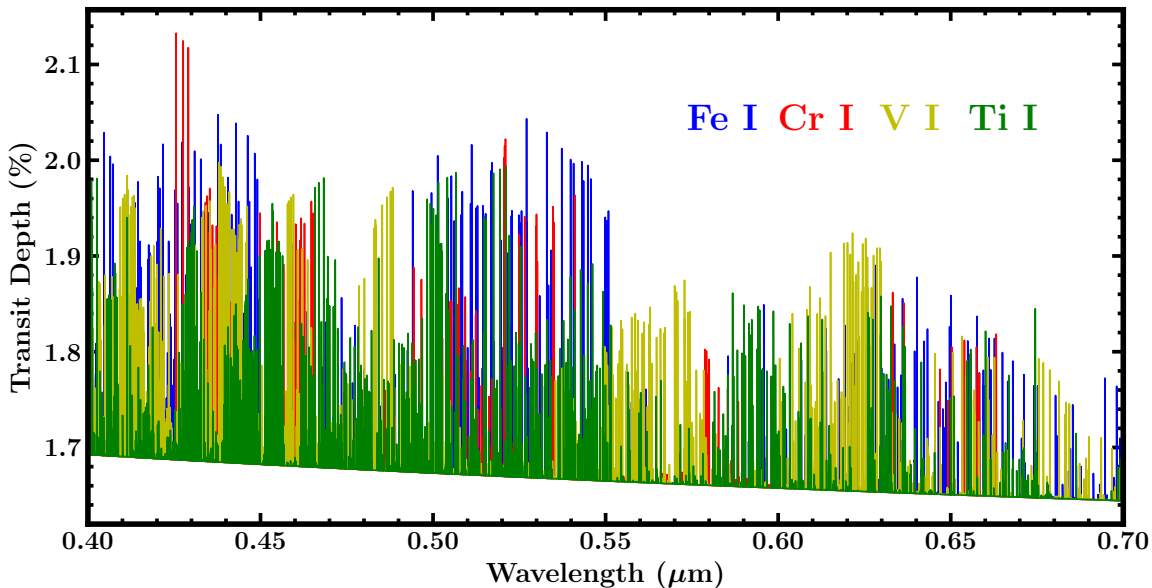


Figure 2. Model transmission spectra of WASP-121 b with contributions from Fe I, Cr I, V I and Ti I. See section 2.3.

analytic models. We compare the numerical models with the analytic models discussed above and find them to be in good agreement.

3. OBSERVATIONS AND ANALYSIS

We demonstrate our predictive methodology on archival transit observations of WASP-121 b. The observations were conducted using the High Accuracy Radial Velocity Planet Searcher (HARPS) spectrograph installed at the ESO La Silla 3.6m telescope, as part of observing programme 0100.C-0750(C) (Hot Exoplanet Atmospheres Resolved with Transit Spectroscopy, PI: D. Ehrenreich). Three transits were observed on nights of 31 December 2017, 09 January 2018, and 14 January 2018 (hereafter Nights 1, 2 and 3). Data were reduced with HARPS DRS v3.8. The extracted 68 orders span 380-690nm at $R \sim 115,000$. Spectra acquired on Night 2 have low signal-to-noise ratio (likely from poor seeing conditions), and are excluded from our analysis. We treat data from Nights 1 and 3 separately in our analysis until computation of detection significances.

3.1. Detrending and Cross-correlation

The majority of our analysis involves common steps in high resolution atmospheric spectroscopy (Snellen et al. 2010; Brogi et al. 2012; Birkby 2018; Hoeijmakers et al. 2019; Casasayas-Barris et al. 2019). We use the X-COR cross-correlation software suite, previously used for molecular detections (Hawker et al. 2018; Cabot et al. 2019) in the near-infrared, and atomic detections

on the present dataset (Cabot et al. 2020). We briefly describe our procedures here as follows; further details can be found in Cabot et al. (2020).

We divide the data by a telluric model, which is fitted and computed by `molecfit` v1.5.7 (Smette et al. 2015). We mask the HARPS chip gap, plus 1% of data from either end of the observed spectrum which are otherwise affected by low throughput or severe telluric contamination. We shift all spectra into the rest-frame of the star by correcting for the planetary-induced radial velocity signal. Next, we construct a master stellar spectrum by co-adding all out-of-transit spectra. Each in-transit spectrum is then divided by the master stellar spectrum. We fit and divide each spectrum by a 5th-degree polynomial, and remove remaining broadband variation with a 75-pixel high-pass filter. We are left with individual transmission spectra (Equation 3) which contain spectral features originating in the planet’s atmosphere. Continuum information was removed in the above normalization.

We form cross-correlation templates by subtracting the continua from the numerical model transmission spectra computed in Section 2.3. We convolve the templates with a narrow Gaussian (FWHM ~ 0.8 km s⁻¹) to approximate the HARPS spectral resolution. The Cross-Correlation Function (CCF) between the model template $m(\lambda)$ and observed transmission spectra $f(\lambda, t)$ is defined as:

$$\text{CCF}(v, t) = \frac{\sum_{\lambda} m(\lambda; v) f(\lambda, t) / \sigma^2(\lambda)}{\sum_{\lambda} m(\lambda; v) / \sigma^2(\lambda)}, \quad (4)$$

	Fe I	Ti I	V I	Cr I	Sc I	Na I	Y I	Ca I	K I	Zr I	Mn I	Sr I	Mg I	Ni I
N_{lines}	185	156	149	71	29	8	30	22	9	28	12	4	2	1
S/N_{av}	1.4	1.28	1.29	1.4	1.32	2.44	1.25	1.39	2.06	1.07	1.57	1.38	1.74	1.18
Ψ	19.02	16.03	15.78	11.81	7.12	6.91	6.85	6.5	6.17	5.68	5.45	2.75	2.45	1.18

Table 1. Detectability metric (Ψ) with $\xi = 2000$ ppm for various neutral atomic species with strong lines in the optical as predicted for the transmission spectrum of WASP-121 b (see section 4).

where we weight summation over wavelength bins λ by the inverse of their time-axis variance $\sigma^2(\lambda)$. This step prevents noisy data (e.g. in the former cores of telluric or stellar lines) from dominating the dot-product. The model is Doppler shifted by velocities $-600 \leq v \leq 600$ km s $^{-1}$ in steps of 2 km s $^{-1}$. The planetary atmospheric signal manifests as a light trail in the CCF, tracing velocities which correspond to the radial component of its orbital motion (which varies by ~ 100 km s $^{-1}$ throughout the course of the transit). For species in common with the host star, we also observe a dark trail due to the Rossiter-McLaughlin effect (Cegla et al. 2016); a result of stellar rotation and the planet selectively occulting portions of the star. We correct for the Doppler Shadow as in Cabot et al. (2020). Following Brogi et al. (2012), we stack the CCFs in time for various values of semi-amplitude K_p . Excess signal from stacking under the true K_p , offset by the true systemic velocity V_{sys} , constitutes an atmospheric detection. The final CCFs combine data from Nights 1 and 3.

4. RESULTS

We now use our model spectra to predict the atomic species detectable in the atmosphere of WASP-121 b and then search for them in observed high resolution spectra. We first discuss our model predictions and then present new detections of Cr I and V I, besides confirming previous detections of Fe I and Fe II.

4.1. Model Predictions

Here we use a simple metric to predict the detectability of a given atomic species using high resolution optical transmission spectra of a UHJ. Our metric is guided by the fact that detecting N_{lines} lines using the cross-correlation method boosts the signal-to-noise ratio (S/N) by $\sqrt{N_{\text{lines}}}$ (Birkby 2018). These lines are those that are strong enough to be detectable. The contribution of species j to the spectrum is given by:

$$\Delta\delta_j = \delta_{c+j} - \delta_c,$$

where δ_c and δ_{c+j} are model transmission spectra with just the continuum opacity and that with contribution from the species j , respectively (see Section 2).

We calculate the number of strong lines N_{lines} in this signal by choosing a noise level ξ and discarding all lines

Species	S/N	Weighted Absorption	K_p	V_{sys}
Fe I	6.0	0.11%	196^{+35}_{-11}	35^{+2}_{-1}
Cr I	3.6	0.10%	245^{+15}_{-18}	37^{+2}_{-2}
V I	4.5	0.08%	229^{+20}_{-23}	35^{+2}_{-3}
Fe II	3.6	0.23%	255^{+6}_{-13}	37^{+1}_{-1}

Table 2. Summary of species detected in the atmosphere of WASP-121 b. The S/N corresponds to the peak of CCF in the K_p - V_{sys} plane. The weighted absorption provides a measure of the average line strength.

weaker than ξ . The S/N for a line is given by $\Delta\delta_j/\xi$ for that line. We take into account the strength of these N_{lines} lines by calculating their average S/N, denoted as S/N_{av} . Finally, our metric for assessing the detectability is given by: $\Psi = \sqrt{N_{\text{lines}}} \cdot S/N_{\text{av}}$.

For WASP-121 b, we use this method and the analytic model spectra of 30 neutral atomic species, as described in Section 2, to evaluate their detectability. Here, we adopt a conservative noise-level of $\xi=2000$ ppm at $R = 10^5$. We present the metric for all species with strong lines above the continuum in Table 1. Following these results, in our analysis of observed spectra of WASP-121 b we search for all the species with $N_{\text{lines}} > 25$: Fe I, Ti I, V I, Cr I, Sc I, Y I and Zr I. These are the species we predict to be likely detectable in the transmission spectra of WASP-121 b, with Fe I, Ti I, V I, and Cr I being the four most likely. We note that this metric is only applicable to the species we expect to find under equilibrium conditions, typically seen in the lower atmosphere.

4.2. Chemical Detections

Based on the predictions above we search for neutral and singly ionised Fe, V, Cr, Ti, Sc, Y and Zr in WASP-121 b using high resolution optical transmission spectra as discussed in section 3. The detections from our cross-correlation analyses are shown in Figure 3. We report new detections of V I with 4.5σ and Cr I with 3.6σ significance, and confirm the previous detection of neutral Fe at 6.0σ significance (Bourrier et al. 2020; Cabot et al. 2020; Gibson et al. 2020). We find no significant excess signal in the cross-correlation functions of Ti I, Sc I, Y I or Zr I. We also report a detection of Fe II in the optical, confirming its previous detection by Sing et al. (2019) in the UV. The weights in the CCF in Equation 4 are not

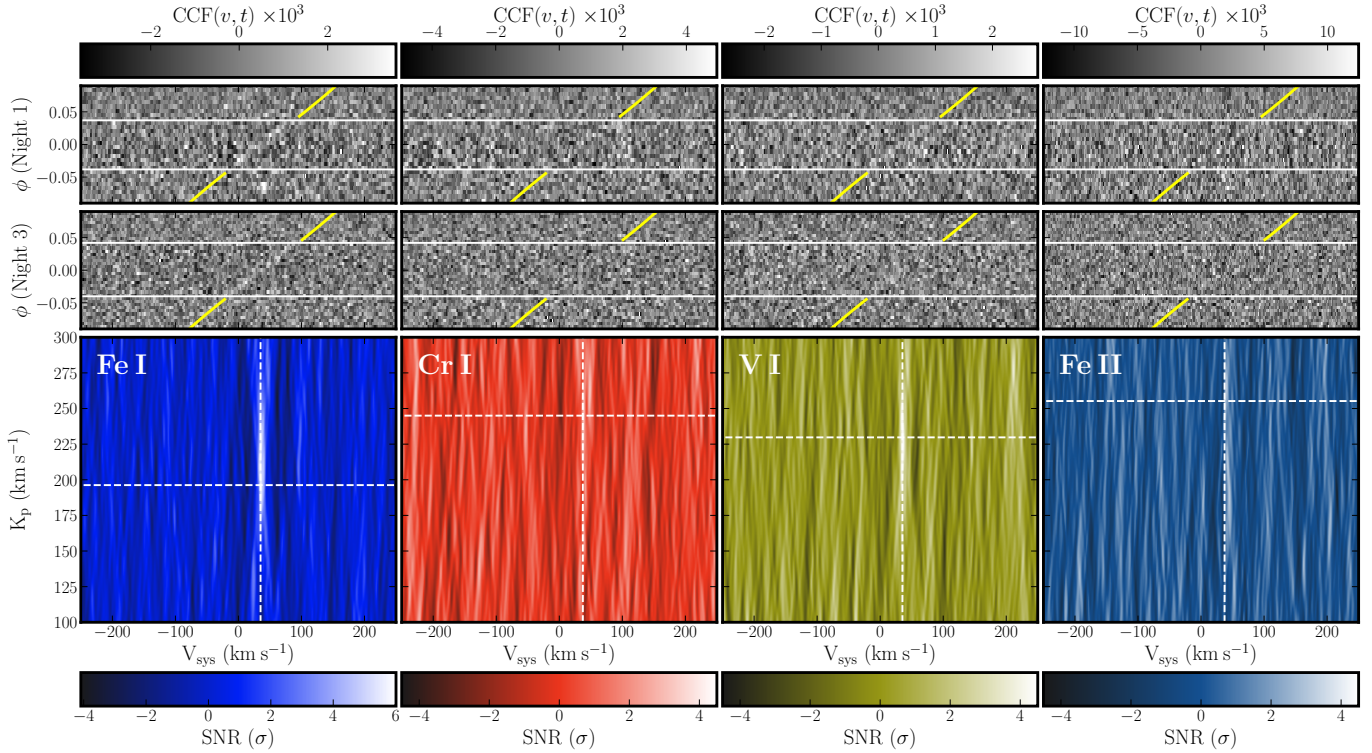


Figure 3. Detection of chemical species in WASP-121 b. *Top gray panels:* CCF in orbital phase and velocity. Horizontal white lines mark the transition between out-of-transit and in-transit. A yellow solid line shows the expected radial velocity of the planet in the out-of-transit frames. *Bottom color panels:* CCF in the K_p - V_{sys} plane for different species; see section 4. Dashed white lines indicate the peak CCF value. We report detections of Cr I and V I, and confirm previous detections of Fe I and Fe II.

optimized for model injection and recovery (Hoeijmakers et al. 2019). As such, our quoted detection significances represent conservative estimates.

The K_p and V_{sys} values derived from the detected planetary absorption signals are consistent, within $1 - 2\sigma$, with the true values of $K_p = 217 \pm 19 \text{ km s}^{-1}$ and $V_{\text{sys}} = 38.350 \pm 0.021 \text{ km s}^{-1}$ (Delrez et al. 2016). Our measurements of K_p and V_{sys} are listed in Table 2. Our detections of neutral species exhibit blueshifts between $1 - 3 \text{ km s}^{-1}$ at a $\lesssim 2\sigma$ level. This may be explained by wind speeds in the photosphere, as inferred in other hot Jupiter atmospheres (e.g., Louden & Wheatley 2015) and predicted by models of atmospheric dynamics (Showman et al. 2009; Miller-Ricci Kempton & Rauscher 2012). The large spread in K_p results from sampling a small portion of the planet’s full orbit (Brogi et al. 2018).

We estimate the neutral Fe, Cr and V to pertain to lower regions in the atmosphere relative to Fe II. The weighted absorption (Hoeijmakers et al. 2019) by neutral species corresponds to ~ 1.02 to $1.04R_p$, whereas Fe II extends to $\sim 1.07R_p$. For a scale height of $\sim 1000 \text{ km}$ (Evans et al. 2018), and nominal pressure of 0.1 bar at the base of the atmosphere (Welbanks & Madhusudhan

2019), the neutral species lie at altitudes corresponding to 3×10^{-3} to 9×10^{-4} bar. For comparison, the stratosphere (Evans et al. 2017) corresponds to approximately 10^{-2} to 10^{-4} bar. On the other hand, we infer Fe II to be present in the upper atmosphere ($\sim 6 \times 10^{-6}$ bar) suggesting it originates in photoionisation of Fe I in agreement with Sing et al. (2019).

The detections we report and the order of their significances are consistent with our predictions. However, we do not detect Ti I even though its predicted detectability (Ψ) is similar to V I. This suggests that Ti I is depleted in the observable atmosphere relative to the solar abundance assumed when calculating Ψ . We estimate the Ti I abundance to be at least $10\times$ below the solar abundance value for its detectability to fall below our threshold.

5. SUMMARY AND DISCUSSION

We report new detections of V I and Cr I in the atmosphere of WASP-121 b at 4.5σ and 3.6σ , respectively, for the first time in an exoplanet. We also confirm previous detections of Fe I in the visible and Fe II in UV. Based on their weighted absorption strengths, we infer the neutral species (Fe I, V I, and Cr I) to pertain to the

lower atmosphere and the ionic Fe II to be in the upper atmosphere. Our study also demonstrates a viable metric to systematically predict the detectability of atomic species in UHJs.

These detections provide important constraints on the chemical and physical processes in the atmosphere of WASP-121 b. Transition metals (e.g., Ti, V, Fe), in both atomic and molecular forms, are known to be strong sources of optical opacity (Fortney et al. 2008; Lothringer et al. 2020) which can influence radiative processes in UHJ atmospheres. The presence of Fe I, V I and Cr I in the lower atmosphere may, therefore, provide the strong optical opacity required to explain the thermal inversion inferred in WASP-121 b (Evans et al. 2017; Gibson et al. 2020; Lothringer et al. 2020). Our detection of V I argues for the thermal dissociation of VO in the observable atmosphere thereby explaining its non-detection in recent searches (Merritt et al. 2020). Our non-detection of atomic Ti despite its strong detectability suggests it is present as molecular TiO which may be condensed out at the terminator.

These results also mark a significant development in our ability to find trace metals in the lower atmospheres

of giant exoplanets. Both Cr and V are trace metals with solar abundances of 0.4 ppm and 0.008 ppm, respectively; two orders of magnitude lower than Fe (30 ppm). While previous searches suggested hints of these species in other UHJs (Hoeijmakers et al. 2019; Cauley et al. 2019), conclusive detections of the same remained elusive. Detecting such species is particularly important considering that they cannot be observed in planets cooler than ~ 2000 K, including solar system giant planets. As such, they provide unique probes of the possibly rich diversity of refractory compositions of giant planets.

Our study highlights the power of high resolution spectroscopy to probe the metal compositions of UHJs, down to temperatures of ~ 2000 K. The detections of five metal species (Na, Mg, Fe, Cr, V) in WASP-121b, which is at the cooler end of UHJs, implies that a wide range of UHJs could be exquisite laboratories for studying a plethora of such elements.

This research has made use of the services of the ESO Science Archive Facility. The study was based on observations collected at the European Southern Observatory under ESO programme 0100.C-0750(C). We thank the anonymous referee for their helpful comments.

REFERENCES

- Asplund, M., Grevesse, N., Sauval, A. J., & Scott, P. 2009, *Annual Review of Astronomy and Astrophysics*, 47, 481
- Bétrémieux, Y., & Swain, M. R. 2017, *MNRAS*, 467, 2834
- Birkby, J. L. 2018, *Spectroscopic Direct Detection of Exoplanets*. Springer International Publishing, Cham, pp 1485–1508
- Bourrier, V., Ehrenreich, D., Lendl, M., et al. 2020, *A&A*, 635, A205
- Brogi, M., Giacobbe, P., Guilluy, G., et al. 2018, *A&A*, 615, A16
- Brogi, M., Snellen, I. A. G., de Kok, R. J., et al. 2012, *Nature*, 486, 502
- Cabot, S. H. C., Madhusudhan, N., Hawker, G. A., & Gandhi, S. 2019, *MNRAS*, 482, 4422
- Cabot, S. H. C., Madhusudhan, N., Welbanks, L., Piette, A., & Gandhi, S. 2020, *MNRAS*, 494, 363
- Casasayas-Barris, N., Pallé, E., Yan, F., et al. 2019, *A&A*, 628, A9
- Cauley, P. W., Shkolnik, E. L., Ilyin, I., et al. 2019, *AJ*, 157, 69
- Cegla, H. M., Lovis, C., Bourrier, V., et al. 2016, *A&A*, 588, A127
- de Wit, J., & Seager, S. 2013, *Science*, 342, 1473
- Delrez, L., Santerne, A., Almenara, J. M., et al. 2016, *MNRAS*, 458, 4025
- Ehrenreich, D., Bourrier, V., Wheatley, P. J., et al. 2015, *Nature*, 522, 459
- Ehrenreich, D., Lovis, C., Allart, R., et al. 2020, *Nature*, 580, 597
- Evans, T. M., Sing, D. K., Kataria, T., et al. 2017, *Nature*, 548, 58
- Evans, T. M., Sing, D. K., Goyal, J. M., et al. 2018, *AJ*, 156, 283
- Fortney, J. J., Lodders, K., Marley, M. S., & Freedman, R. S. 2008, *ApJ*, 678, 1419
- Gandhi, S., & Madhusudhan, N. 2017, *MNRAS*, 472, 2334
- . 2019, *MNRAS*, 485, 5817
- Gibson, N. P., Merritt, S., Nugroho, S. K., et al. 2020, *MNRAS*, 493, 2215
- Harrison, J. H. D., Bonsor, A., & Madhusudhan, N. 2018, *MNRAS*, 479, 3814
- Hawker, G. A., Madhusudhan, N., Cabot, S. H. C., & Gandhi, S. 2018, *ApJ*, 863, L11
- Haynes, K., Mandell, A. M., Madhusudhan, N., Deming, D., & Knutson, H. 2015, *ApJ*, 806, 146
- Hoeijmakers, H. J., Ehrenreich, D., Heng, K., et al. 2018, *Nature*, 560, 453

- Hoeijmakers, H. J., Ehrenreich, D., Kitzmann, D., et al. 2019, *A&A*, 627, A165
- Hoeijmakers, H. J., Cabot, S. H. C., Zhao, L., et al. 2020, arXiv e-prints, arXiv:2004.08415
- Kitzmann, D., Heng, K., Rimmer, P. B., et al. 2018, *ApJ*, 863, 183
- Kramida, A., Ralchenko, Y., Nave, G., & Reader, J. 2018, in *APS Meeting Abstracts*, Vol. 2018, APS Division of Atomic, Molecular and Optical Physics Meeting Abstracts, M01.004
- Kurucz, R. L. 2018, *Astronomical Society of the Pacific Conference Series*, Vol. 515, Including All the Lines: Data Releases for Spectra and Opacities through 2017, 47
- Lecavelier Des Etangs, A., Pont, F., Vidal-Madjar, A., & Sing, D. 2008, *A&A*, 481, L83
- Lothringer, J. D., Barman, T., & Koskinen, T. 2018, *ApJ*, 866, 27
- Lothringer, J. D., Fu, G., Sing, D. K., & Barman, T. S. 2020, arXiv e-prints, arXiv:2005.02528
- Louden, T., & Wheatley, P. J. 2015, *ApJL*, 814, L24
- Merritt, S. R., Gibson, N. P., Nugroho, S. K., et al. 2020, *A&A*, 636, A117
- Mikal-Evans, T., Sing, D. K., Goyal, J. M., et al. 2019, *MNRAS*, 488, 2222
- Miller-Ricci Kempton, E., & Rauscher, E. 2012, *ApJ*, 751, 117
- Nugroho, S. K., Gibson, N. P., de Mooij, E. J. W., et al. 2020, arXiv e-prints, arXiv:2003.04856
- Parmentier, V., Showman, A. P., & Lian, Y. 2013, *A&A*, 558, A91
- Parmentier, V., Line, M. R., Bean, J. L., et al. 2018, *A&A*, 617, A110
- Pinhas, A., Rackham, B. V., Madhusudhan, N., & Apai, D. 2018, *MNRAS*, 480, 5314
- Richard, C., Gordon, I., Rothman, L., et al. 2012, *Journal of Quantitative Spectroscopy and Radiative Transfer*, 113, 1276, three Leaders in Spectroscopy. <http://www.sciencedirect.com/science/article/pii/S0022407311003773>
- Showman, A. P., Fortney, J. J., Lian, Y., et al. 2009, *ApJ*, 699, 564
- Sing, D. K., Lavvas, P., Ballester, G. E., et al. 2019, *AJ*, 158, 91
- Smette, A., Sana, H., Noll, S., et al. 2015, *A&A*, 576, A77
- Snellen, I. A. G., de Kok, R. J., de Mooij, E. J. W., & Albrecht, S. 2010, *Nature*, 465, 1049
- Stangret, M., Casasayas-Barris, N., Pallé, E., et al. 2020, arXiv e-prints, arXiv:2003.04650
- Turner, J. D., de Mooij, E. J. W., Jayawardhana, R., et al. 2020, *ApJL*, 888, L13
- Welbanks, L., & Madhusudhan, N. 2019, *AJ*, 157, 206
- Wong, I., Shporer, A., Morris, B. M., et al. 2019, arXiv e-prints, arXiv:1910.01607
- Wytenbach, A., Ehrenreich, D., Lovis, C., Udry, S., & Pepe, F. 2015, *A&A*, 577, A62
- Yan, F., & Henning, T. 2018, *Nature Astronomy*, 2, 714
- Yan, F., Casasayas-Barris, N., Molaverdikhani, K., et al. 2019, *A&A*, 632, A69